A Survey of Jet Aircraft PM by TEM in APEX III

Randy L. Vander Wal
Penn State University, University Park, Pennsylvania

Victoria M. Bryg
The Universities Space Research Association
National Center for Space Exploration Research, Cleveland, Ohio

NASA STI Program . . . in Profile

Since its founding, NASA has been dedicated to the advancement of aeronautics and space science. The NASA Scientific and Technical Information (STI) program plays a key part in helping NASA maintain this important role.

The NASA STI Program operates under the auspices of the Agency Chief Information Officer. It collects, organizes, provides for archiving, and disseminates NASA's STI. The NASA STI program provides access to the NASA Aeronautics and Space Database and its public interface, the NASA Technical Reports Server, thus providing one of the largest collections of aeronautical and space science STI in the world. Results are published in both non-NASA channels and by NASA in the NASA STI Report Series, which includes the following report types:

- TECHNICAL PUBLICATION. Reports of completed research or a major significant phase of research that present the results of NASA programs and include extensive data or theoretical analysis. Includes compilations of significant scientific and technical data and information deemed to be of continuing reference value. NASA counterpart of peer-reviewed formal professional papers but has less stringent limitations on manuscript length and extent of graphic presentations.

- TECHNICAL MEMORANDUM. Scientific and technical findings that are preliminary or of specialized interest, e.g., quick release reports, working papers, and bibliographies that contain minimal annotation. Does not contain extensive analysis.

- CONTRACTOR REPORT. Scientific and technical findings by NASA-sponsored contractors and grantees.

- CONFERENCE PUBLICATION. Collected papers from scientific and technical conferences, symposia, seminars, or other meetings sponsored or cosponsored by NASA.

- SPECIAL PUBLICATION. Scientific, technical, or historical information from NASA programs, projects, and missions, often concerned with subjects having substantial public interest.

- TECHNICAL TRANSLATION. English-language translations of foreign scientific and technical material pertinent to NASA's mission.

Specialized services also include creating custom thesauri, building customized databases, organizing and publishing research results.

For more information about the NASA STI program, see the following:

- Access the NASA STI program home page at *http://www.sti.nasa.gov*

- E-mail your question to *help@sti.nasa.gov*

- Fax your question to the NASA STI Information Desk at 443–757–5803

- Phone the NASA STI Information Desk at 443–757–5802

- Write to:
  STI Information Desk
  NASA Center for AeroSpace Information
  7115 Standard Drive
  Hanover, MD 21076–1320
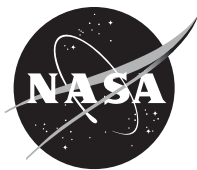
A Survey of Jet Aircraft PM by TEM in APEX III

Randy L. Vander Wal
Penn State University, University Park, Pennsylvania

Victoria M. Bryg
The Universities Space Research Association
National Center for Space Exploration Research, Cleveland, Ohio

National Aeronautics and
Space Administration

Glenn Research Center
Cleveland, Ohio 44135

June 2014

Acknowledgments

Level of Review: This material has been technically reviewed by NASA technical management OR expert reviewer(s).

Available from

A Survey of Jet Aircraft PM by TEM in APEX III

Randy L. Vander Wal
Penn State University
University Park, Pennsylvania 16802

Victoria M. Bryg
The Universities Space Research Association
National Center for Space Exploration Research
Cleveland, Ohio 44135

Abstract

Based upon field testing during the NASA led APEX III campaign conducted in November 2005 at the NASA Glenn Research Center in coordination with Continental Airlines and Cleveland Hopkins International Airport. This paper reports observations of particulate emissions collected from a suite of jet engine aircraft to assess differences and similarities in soot macro- micro- and nanostructure using transmission electron microscopy (TEM). Aggregates are compact, primary particle sizes varied and nanostructure mixed. Comparisons are made to more familiar laboratory flame-generated soot as a well-studied point of reference. Results are interpreted in terms of turbulence interacting with the different stages of particle formation and growth.

Introduction

This paper reports differences in soot structure across a variety of jet engines on different aircraft. The purpose is to identify commonalities of structure across length scales and differences relative to laboratory-generated soot. Different studies have suggested suitability of lab-generated soots as surrogates (Popovitcheva et al. 2000; Karcher et al. 2007), but comparative metrics between the two, such as physical structure are absent. This article reports such, using transmission electron microscopy (TEM) to compare across a range of spatial scales for soot produced by a variety of jet engines, as a first such survey. Such results can provide a baseline for future reference.

Prior studies of jet aircraft PM emissions have shown but a few low magnification images of collected particulate, but generally lacking detailed examination, certainly of nanostructure. The most definitive illustration is that by Popovicheva et al. (2003), who reported crystalline structure within the particles near to the combustor exit (~10 cm), but loss of crystalline structure and coalescence of morphology farther downstream (~100 cm). Though produced with similar overall equivalence ratio as at cruise conditions, gaseous fuels were used in the surrogate combustor, absent design details. High resolution TEM and comparisons at any magnification, either across power, fuels or engine class was absent. Such mutability for the conditions used warrants further observations.

More recently extensive aerosol measurements have been applied to characterize exhaust emissions in a series of field campaigns, APEX I, II, III, AAFEX I, II and in engine test stands (Kinsey and Hays 2011; Vander Wal et al. 2013; Huang and Vander Wal 2013). Related techniques have included scanning mobility particle sizer/condensation particle counter (SMPS/CPC), multi-angle absorption photometer (MAAPs), engine exhaust particle sizer (EEPS) and comparative smoke number measurements.

From these, key results such as particle number concentrations, aerodynamic size distributions were found. With assumptions of sphericity and unit mass density, mass per unit fuel consumed yield particle number and mass emission indices (Corporan et al. 2007; Herndon et al. 2005; Schmid et al. 2004; Wey et al. 2007; Timko et al. 2010). A common trend is that emission indices in both particle number and mass (each per unit fuel consumed) across a series of engines exhibit minima at intermediate powers and steep increases at both low and high powers (Timko et al. 2010).

TEM is particularly valuable in that it provides directly observable physical structure on multiple length scales, as relevant to environmental processes and health impacts. In recent years image analysis algorithms have advanced sufficiently so as to quantify such data (Yehliu 2010; Vander Wal et al. 2011; Yehliu et al. 2011; Teini et al. 2011). By examining several such images, statistical analyses of structure at varied length scales can be made, ranging from nano- to micro- to macro-structure (Vander Wal et al. 2013; Huang and Vander Wal 2013; Wey et al. 2006). For soot, these length scales pertain to carbon lamellae, primary particle size and aggregate morphology, respectively. Each spatial scale is relevant to primary particle formation and growth.

These same length scales are also relevant to the environmental impact of soot. Jet aircraft contribute significantly to soot in the upper troposphere and at ground level near airports (Bond et al. 2004; Hagen and Whitefield 1996; Penner et al. 1999). Soot aggregate physical size and surface chemistry have direct consequences for atmospheric processes (Wuebbles et al. 2007). Soot surface chemistry determines its propensity to act as cloud condensation nuclei (CCN) as does its hydrophobic/hydrophilic balance for coalescence with inorganics (Khalizov et al. 2009). In turn soot surface chemistry depends upon nanostructure (Popovitcheva et al. 2003). Aggregate size and morphology are also relevant to the light absorption and scattering properties, and hence soot's radiative forcing (Liu and Smallwood 2009; Li et al. 2010). Aggregate size and surface chemistry also determine atmospheric longevity (Riemer et al. 2004).

Understanding soot aggregate size, morphology, surface chemistry and related consequences requires direct and detailed examination of soot from gas turbine engines and high-pressure combustors operating under realistic conditions. For this purpose, observations are reported as the first, as known to the authors, across engines for physical structure and particle composition, to fill knowledge gaps regarding these soot characteristics. The data are not presented as a comparison between engines or as a function of power level. Observed soot structure is interpreted as reflective of the turbulent, fuel rich environment. This knowledge has the potential to contribute to future modeling of soot growth in the non-uniform, fuel-rich regions within high-pressure gas turbine engines (Bisetti et al. 2012).

Experimental

The engines and aircraft in the field campaign are summarized in Table 1. Operational jet aircraft were temporarily loaned by Continental Airlines, in coordination with the Cleveland Hopkins International Airport. Soot from these engines was generally sampled at high power, typically 85 percent or 100 percent of full power. Fuel for all jets was commercial Jet-A. These and lower powers were studied by gas analyzers and varied particle analysis instruments, by other groups. These results are to yet be summarized in a future NASA TM. These powers correspond to take-off conditions and are those associated with the majority of near-ground level PM emission, and correspond to the data/samples collected using a custom sampling probe.

Soot entrained within the exhaust was sampled directly upon a TEM grid (Vander Wal et al. 1995). As shown in Figure 1 the probe held a TEM grid within the flow, and was inserted into a swagelock tee for convenience of plumbing into exhaust lines. Essentially it is a 1/4 in. brass rod, approximately 5 cm in length with set screw to hold a folded brass clip made from 0.005 in. shim stock. Folded, it retains the TEM grid with exposure provided by the 2 mm hole near its end, as shown. The swagelock tee provides ease of insert and also a gas-tight seal around the brass rod of standard rod diameter. The key advantage to our collection during the APEX campaign was the direct collection of the soot from the aerosol phase. This bypasses filter collection with the need for re-dispersal upon a TEM grid. Such processes inherently lose aggregate distinction through agglomeration. Soot was collected upon the grid during the entire test duration, typically limited to a few minutes or less when running at full power, for reasons of engine

TABLE 1.—THE OPERATIONAL JET AIRCRAFT AND THE TESTED ENGINES

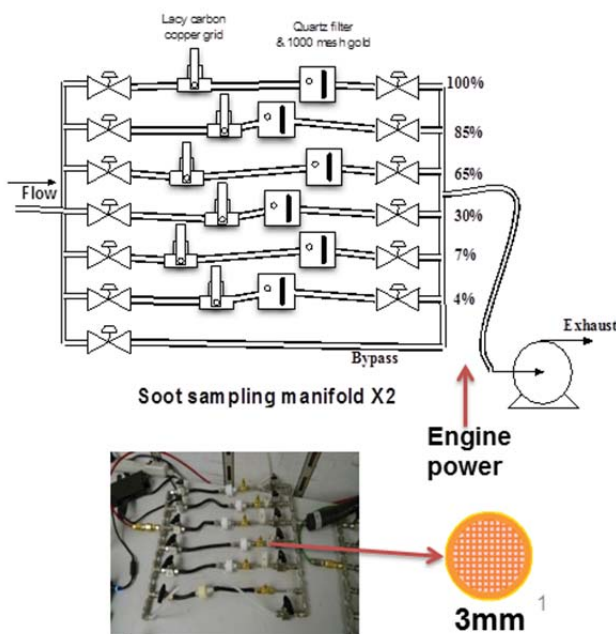| Aircraft	B737-700	Lear 25	ERJ	A300-600
Engine	CFM56-3	CJ610	145-XRJ/AE3007	PW4158
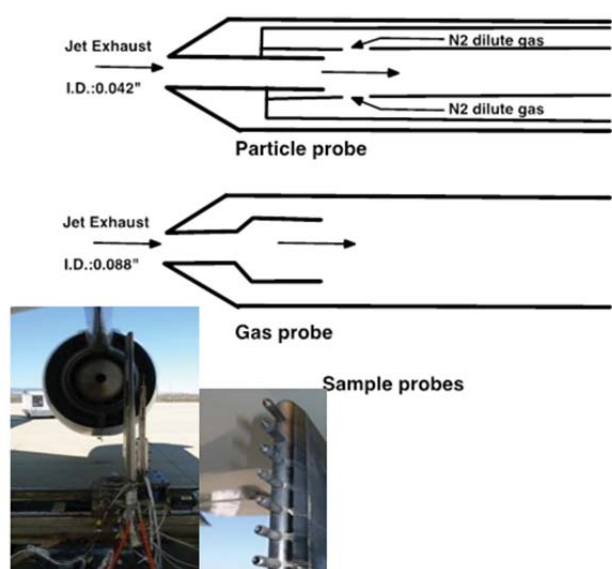
Figure 1.—The schematics of the (L) sample probes: particle and gas probes; (R) soot sampling manifold.

cooling requirements. Complimentary samples include soot collected on quartz fiber filters, which were included in the direct sampling line for quantification of soot concentration by absorption measurements which were retained for subsequent XPS characterization, to be reported elsewhere (Vander Wal and Bryg 2013).

All jet aircraft were fueled by JP-A. Run times varied depending upon the power level. (For experimental reasons related to engine cooling, the A300 aircraft was not run at 100 percent power). Multi-port particle sample rakes were designed, built, and successfully deployed to sample the exhaust plume at 1 and 10 m downstream of the engine exhaust plane. Collection at the 10 m sampling position was not tip-diluted. Streams, diluted 10:1 with ambient air were transferred through about 30 m of heated (177 °C) sampling line (12.7 mm I.D.) to individual instruments through a distribution manifold. Residence time within the sampling systems was less than 10 s, which is within the SAE Aerospace Recommended Practice (ARP 1256B) limits.

The normal diffusion flame was established on a Santoro-style burner, with ethylene as fuel. The fuel flow rate was 238 sccm through a center brass tube of 10.1 mm I.D. with an air co-flow of 43.2 slm through a surrounding honeycomb (Santoro et al. 1983). This flame has become the defacto system for studying soot processes. Further details for the laboratory flame and sampling system have been described elsewhere (Vander Wal 1997).

Given the predominant soot literature based upon laboratory flames, typical data, in the form of TEM images is presented for comparison. It is not unique nor is it suggested by such illustration that such a system can serve as surrogate for the jet engine. However, commonality of flame-produced particulate, if observed would suggest relevance of formation, growth and oxidation studies to jet engine formed soot.

To access soot aggregate size, shape and internal nanostructure, HRTEM was applied. (The TEM was performed in a Phillips CM20 operating at a nominal 200 keV using a LaB6 filament.) Gatan software, v. 3.4, was used for microscope operation. Post-processing of images included analysis of geometric descriptors using the software package Optimus and ImageJ. Custom analysis algorithms developed on the Optimus platform provided quantification of nanostructure metrics, such as lamella length. Generally 3 to 6 areas were examined upon the grid, with images at a series of magnifications taken at 3 or more locations. Images shown here are judged qualitatively representative.

Results

Macrostructure

To test the suitability of lab-generated soot as a surrogate for jet engine PM as cited elsewhere (Popovitcheva et al. 2003; Demirdjian et al. 2007), Figure 2 shows a typical soot aggregate from the laminar diffusion flame. The varied magnifications illustrate the relevant length scales. Many other similar images from the same flame have been reported elsewhere (Koylu et al. 1994; Koylu et al. 1995). As seen by comparison of the images shown in Figure 3, the open, branched structure so often describing flame-produced soot appears largely inapplicable to soot from jet engines. Aggregates are compacted, somewhat elongated. Few gaps and little void volume are evident between primary particles, as particularly exemplified by the Lear jet soot. Such compact morphology is suggestive of locally ballistic (primary) particle aggregation, as would be possible with a high (primary) particle concentration (Shim et al. 2000). Figure 4 shows the examination of soots from the B737 aircraft at 4 and 65 percent power suggest similar morphology. No observable coating or amorphous liquid-like coating was found on the particles.
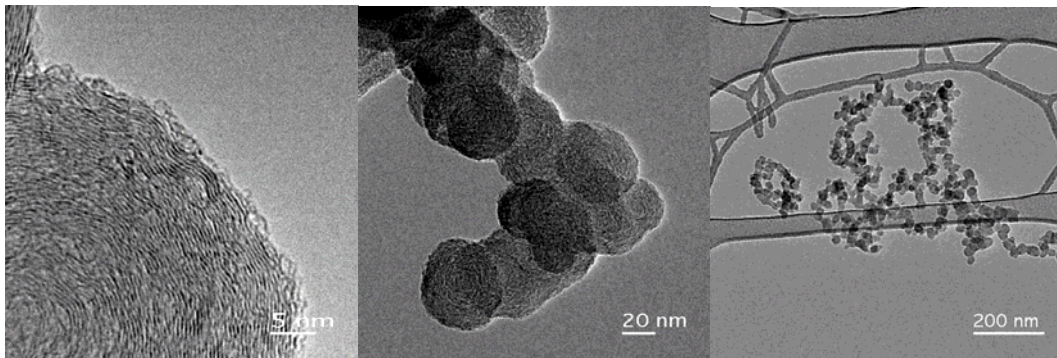

Figure 2.—TEM images at the indicated magnifications of soot sampled from an ethylene gas jet diffusion flame at atmospheric pressure, illustrating varied length scales.
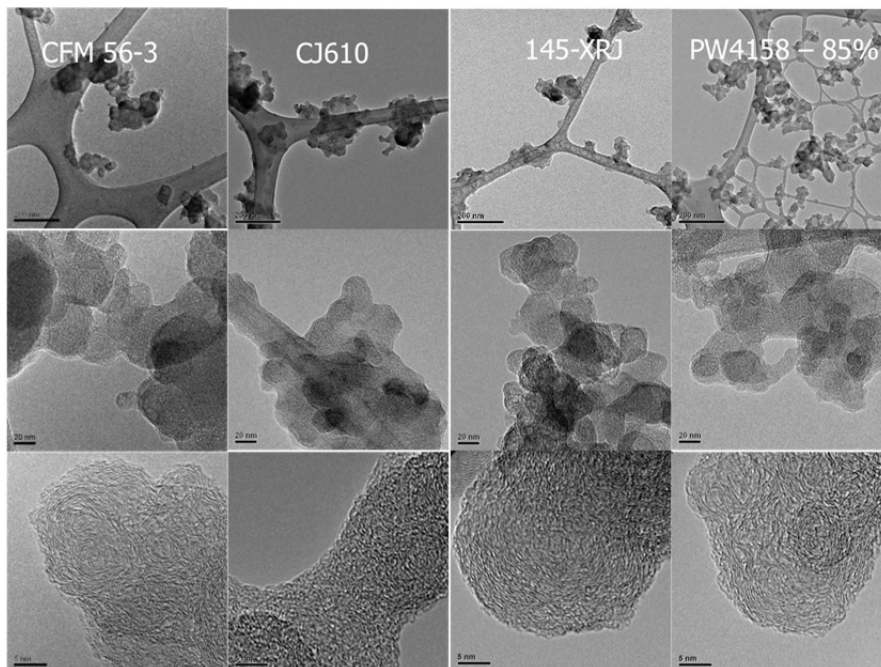

Figure 3.—TEM images at successive magnifications of the soots produced by the different aircraft, each at 100 percent power (except where noted). (From left to right = CFM 56-3; CJ610; 145-XRJ; PW4158—85 percent.)
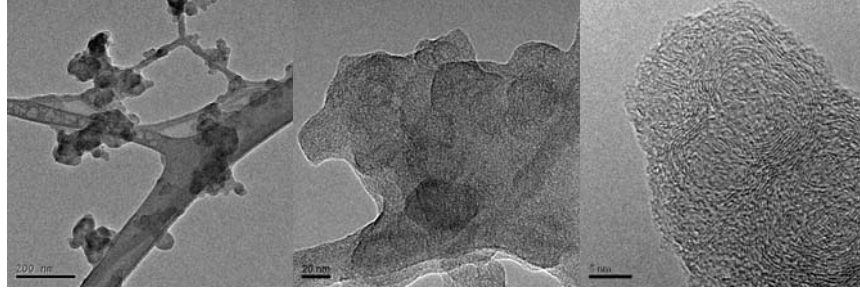
Figure 4.—TEM images at successive magnifications of the soots produced by B737 at 4 percent (top row) and 65 percent (bottom row) power levels.

Two foremost differences are the fuel and combustion system, being a high pressure, liquid-fueled gas turbine. Moreover multiple injectors are often present and recirculation is inherent to designs to achieve flame stability. Wall flow cooling further alters the aerodynamics, hence simple interpretations of monotonic temperature or equivalence ratio, ϕ, with time, as along the center streamline of a lab-scale gas jet flame are void. Further complicating comparisons are temperature and pressure differences between engines and varied power levels. With paucity of TEM reports but decided impact upon atmospheric processes, a survey is presented of results across engines at power levels relevant to take-off and cruise operation for comparison of structural similarities and differences between the aircraft platforms.

As observed for the jet soots, aggregates exhibit a more compact morphology. This is often qualitatively observed in soots from other practical combustion sources such as engines, producing soot under conditions of elevated pressure. Yet quantitatively distinguishing such differences is difficult, as the fractal dimension varies little between quite distinct morphologies. Across the different jet soots, the fractal dimension varies between 1.6 and 1.8, less than a 12 percent variation. Therein alternative geometric measures were investigated to characterize and quantify the morphologies. The formulas are summarized in Table 2. These metrics are commonly used for morphological analysis of objects within images (ImageJ 1997). Numerical results for these geometric measures applied to the different soots are shown in the bar graph plots of Figure 5. For illustrative comparisons, two soots from the B737 at widely different powers (100 and 56 percent) are compared to soots from the Lear and ERJ aircraft, each at full power. Results are presented for engines and power levels for which sufficient data existed to permit analysis of greater than 20 aggregates for each engine and power level.

As observed from the plots in Figure 5, aspect ratio exhibit a minimal variation of < 20 percent with roundness showing a similar range. Compactness, a measure of overall asymmetry provides even less difference (< 10 percent). By recognizing the importance of irregular boundaries, the root form factor well describes differences in morphology with nearly a 2.5-fold (250 percent) variation between sampled aggregates, suggesting it to be the superior metric of morphology, and subtle variations. By contrast the aggregates from the ND flame possess an average fractal dimension of 1.74 and pre-factor of 2.2 (Hu et al. 2003).

These values can be compared to those found by fractal analysis, which exhibit a minimal range, generally from 1.6 to 1.8, as routinely reported for soot aggregates from both engines (Lind et al. 2010) and laboratory flames (Gangopadhyay et al. 1991)—traditionally interpreted as reflecting similarity of soot (aerosol) processes. The purpose for comparison of geometric measures is not to suggest that these particular values represent the different PM emissions from these jet engines but rather to use these varied (real) sources to identify a geometric measure that is more sensitive to morphology differences—visually evident (by TEM) across the array of engines. A larger dynamic range, as found in the root form factor has this potential for compact aggregate morphologies found here, a characteristic of soots produced by high pressure combustion (Zhu et al. 2005).

TABLE 2.—FORMULAS FOR DIFFERENT GEOMETRIC DESCRIPTORS OF
SOOT AGGREGATE MORPHOLOGY

Geometric description	Formulas
Root form factor	$\dfrac{\sqrt{4\pi}}{Perimeter^2}$
Aspect ratio	$\dfrac{x}{y}$
Compactness	$\sqrt{\dfrac{4}{\pi}A}$
Roundness	$\dfrac{4A}{\pi^2 x}$

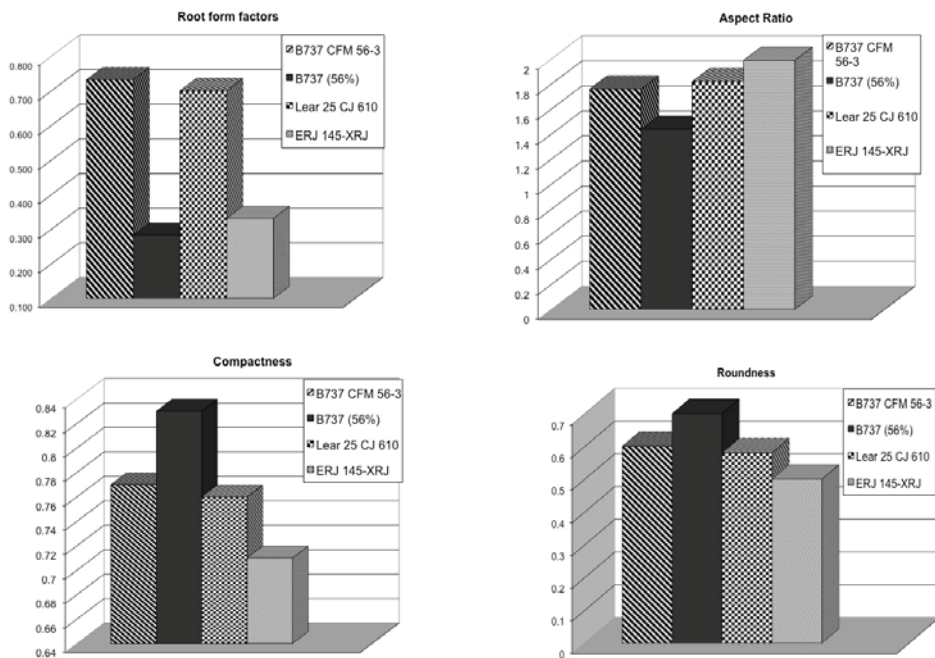x: major axis; y: minor axis; A: area

Figure 5.—Results of geometric descriptors for soot aggregate morphology. Formulas
are indicated in corresponding Table 2.

Aggregate structure bears witness to the aerosol dynamics and mass growth conditions. The degree of fusion between individual spherules serves as a clock of aggregation relative to continued growth (Gaddam and Vander Wal 2013). Two jet soots well illustrate these differences. The A300 soot exhibits a branched structure suggesting late aggregation relative to primary particle growth. By contrast the B737 produces aggregates with tight compaction suggesting just the opposite occurrence. If growth continues well beyond aggregation distinctive substructure is largely lost and only appear, as evident in Figure 3. These can be contrasted with the contacting spherule within the ND flame, as seen in Figure 1. Soot from diffusion flames typically exhibits a central region or core of less structure or even recognizable nuclei, clearly marking stages of coalescence and continued growth (Merchan-Merchan et al. 2012; Zhang and Boehman 2013).

Microstructure

Another striking feature of the aggregates is the disparate primary particle sizes, with highlights in the middle row of images in Figure 3, and the low magnification images (1st column) of Figure 4. For such vastly different sizes to co-exist within the same aggregate is unusual. By analyzing a series of such images, the means of the two primary particle populations are 17 ± 3 and 4 ± 1. These are statistically different by application of the Student's T-test to 99 percent confidence. Either the growth environments were different or the timescales within a given growth region were different to produce such different size classes. Such disparate size classes are not observed in atmospheric pressure, laboratory diffusion flames (Koylu et al. 1994; Koylu et al. 1995). By either process, to come together from different spatial locations requires fast transport as would be facilitated by turbulent mixing (Bisetti et al. 2012), and conjectured here. This is particularly true for the small primary particles that are physically linked to the larger aggregate, and not merely physically adhered as would occur in agglomeration. Notably aggregate collapse to form nodular structures as reported elsewhere was not observed (Popovitcheva et al. 2003), likely reflecting differences in fuel, engines, or sampling procedures.

Nanostructure

Primary particles exhibit divergent nanostructure, as seen in the last image row of Figure 3. For the Lear soot nanostructure appears rather uniform throughout, even more so for the ERJ soot. There is no radial dependence to it nanostructure nor recognizable core within "particles" or substructures. This suggests uniformity of growth environment, species and temperature, and absence of phases associated with primary particle nucleation, coalescence and subsequent growth, as are spatially delineated in an ordinary gas-jet diffusion flame (Dobbins et al. 1996).

This is in contrast to the laboratory-generated soot where a clear radial dependence is observed, characteristic of the temperature and species profile within the laminar diffusion flame (Vander Wal and Tomasek 2003). Along the center streamline in such buoyancy driven flames, precursor particles form, carbonize and further surface mass growth occurs throughout the fuel-rich region (Dobbins et al. 1995; Vander Wal 1998). Such a monotonic traverse in temperature and species is reflected in the nanostructure and its radial variation.

In highly turbulent liquid-fueled combustors, soot (particle) formation may not follow such a model path (Liu and Smallwood 2009; El-Asrag and Menon 2009). The resulting particle nanostructure, specifically core-shell construction would be lost, or at the very least, different. Though seemingly homogeneous, the A300 soot contains amorphous regions and extended lamella interspersed throughout the particle. Irregular growth, particularly as engendered by varied species underlies such assembly. This again is in contrast to the flame soot in which nanostructure is circumferentially uniform (Fig. 1). Uniform structure in the Lear soot suggests no such variation or rather sufficiently rapid formation so as to be insensitive to the timescale on which such changes occur. Oddly the B737 soot shows multiple nucleation centers, indicative of coalescence between multiple precursor particles to form a primary particle. High equivalence ratio at high temperature would be conducive to such formation by fostering a high density of seed nuclei. Based on the TEM image, the primary particle nanostructure reflects ballistic rather than diffusional aerosol dynamics between the soot precursor particles (Chakrabarty 2008). Oddly some particles were either composed of two very different nanostructures (as marked by the divots in Figure 6) or were juxtaposed. Unlike a laminar diffusion flame, non-monotonic temperature and species profiles as imposed by turbulence are interpreted as causative.
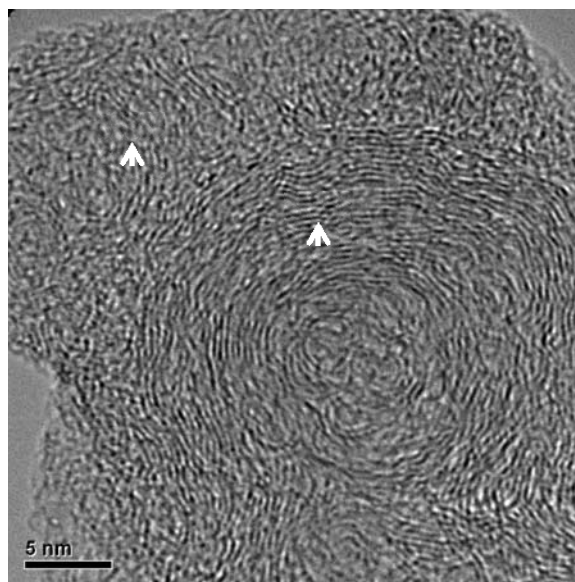
Figure 6.—A HRTEM image of an individual primary particle of the Lear jet soot showing disparate nanostructure with a clear geometric boundary between.

To be noted is that combustion environment or chemical environment refers to both gas-phase and surface molecular re-arrangement processes that drive particle growth (Grieco et al. 2000; Howard and Richter 2000). Both contribute to the observed nanostructure and their differentiation or relative contributions is not the focus here, nor within resolution given "end-product" observations. However both will depend upon species and temperature, and rationale for translation of nanostructure reflecting the chemical growth "environment".

Though sampled from the engine exhaust plume, no evidence was found for extensive surface oxidation. In other studies by HRTEM of partially oxidized soots, whether by TGA or lean diesel operation, primary particles appear with roughened surfaces (Vander Wal and Tomasek 2003) and are readily distinguished. Slower oxidation, such as in diesel particulate traps or via TGA analyses can lead to internal burnout or particle restructuring. No such modes were observed in these exhaust entrained samples.

Given the design and operational differences between engines, results are not compared across platforms but instead presented as a survey of the emitted soot, at high powers relevant to take-off operation. Along with a more compact morphology are less distinct primary particles. Aggregate compactness and loss of substructure reflect necessarily the same aerosol dynamics (Puri et al. 1993). Late coalescence relative to particle growth forms aggregates with an open, branching structure whereas early coalescence followed by continued mass surface growth yields compactly clustered aggregates of primary particles (Slowik et al. 2004). The relative timescales of mass (surface) growth versus coalescence depend upon species concentration and hence pressure, for temperatures sufficient to activate both pyrolysis and free radical generation (Ishiguro et al. 1997). Soot from diffusion flames typically exhibits a central region or core of less structure or even recognizable nuclei, clearly marking stages of coalescence and continued growth (Raj et al. 2010). This is observed in both the laboratory-generated soot and in soot from the 145-XRJ (ERJ) engine.

In both images arrows point to the inner core and outer perimeter of recognizable primary particles, illustrating the contrasting nanostructure. For some of the jet soots, such as from the CFM56-3 engine with low power level, such structure is absent. There is no radial dependence to it nanostructure nor recognizable core within "particles" or substructures. This suggests uniformity of growth environment, species and temperature, and absence of phases associated with primary particle nucleation, coalescence

and subsequent growth, as are spatially delineated in an ordinary gas-jet diffusion flame (Frenklach 2002; Santoro et al. 1983). For the CJ610-engine (Lear) soots, soot formation as judged by particle nanostructure appears to not follow the traditional soot growth stages. This inference does not necessarily pertain to rate of particle formation/growth, only to the homogeneity of formation conditions as judged by uniformity of nanostructure throughout the aggregate and its subsections.

Discussion

Though multi-team programs have comprehensively investigated detailed chemical kinetic models for surrogate fuels (Gudiyella et al. 2011; Gudiyella and Brezinsky 2012), and large-scale CFD models have incorporated soot models (Tolpadi et al. 1997; Colket et al. 2007), experimental measurements are yet needed as reference by which to extend chemical species models to soot nanostructure. As example, present models embody the pre-mixing designed into practical systems and the burning of fuel-rich, partially premixed regions. Above the critical stoichiometry threshold for soot formation, examination of soot under such conditions would be illuminating for the dependence upon mixing of soot structure across all lengths.

More generally a jet engine is designed to burn overall lean with turbulence contributing to the mixing. Within turbulent flames soot particles can pass from regions of growth to oxidation to yet again growth (Vander Wal 1997). Each such region will interact with the soot particle surface but most telling will be multiple growth stages. If the different (growth) regions differ in species and temperature this should be reflected in the nanostructure. As observed in Figure 6, the primary particle shows two distinctly different nanostructures merged together. The broad interface and conformal knit between the two nanostructure types suggests a 2nd stage of growth as opposed to simple physical coalescence between two different primary particles. The absence of a "between particle gap" is consistent with this. Even if the particle shown in Figure 6 were actually two different primary units that physically came together, their varied nanostructure still points to different environments in time and temperature for their formation. This has not been reported for laboratory flames but is quite likely in practical systems. Recent turbulent models of soot within turbulent and flames anchored by recirculation regions include such non-monotonic variation in temperature and time (Bisetti et al. 2012; El-Asrag et al. 2007).

In summary, turbulence breaks up fuel rich regions, lowers their overall equivalence ratio and can even move soot particles between rich and lean regions, in either order. Such shifts in chemical environments create a complicated and non-monotonic particle history by multiple stages of growth and oxidation, of varied temperature and duration (Bisetti et al. 2012). Laboratory studies of this appear absent. We conjecture that soot particle structure across length scales will reflect such histories, as suggested by the variety of soot structures observed here.

Conclusions

Aggregate morphologies attest to aerosol dynamics, at high pressure. Reaction-limited aggregation leads to tight clusters whereas diffusion limited, particle-cluster aggregation is more representative of atmospheric pressure soot. Turbulence interacts by mixing particles from different growth trajectories. The large range of primary particle sizes is indicative of varied nucleation and growth environments. Nanostructure is indicative of species and temperature. Differences point to formation in regions of significantly different temperature and species so as to be manifest in the soot structure, at all length scales. Turbulence mixing is considered the operative factor for crossing particle trajectories from varied spatial regions. Models of PM formation in turbulent environments will need to include such variations for accurate prediction.

Though lacking the model macro-, micro- and nanostructure of model flame soot, on all levels these physical scales appears similar to soot produced under other high pressure, rapid timescale engines, such as diesel despite vast differences in design, combustion conditions and fuels.

The familiar model system, a laboratory scale gas-jet diffusion flame is very fuel-rich throughout the particle formation and nucleation regions. Such flames do not encompass the timescales and pressures of operation within engines and combustors. Indeed earlier studies of aircraft engine soot suggest substantial differences (Anderson et al. 2011). Yet other studies claim adequacy of laboratory-generated soots as surrogates (Popovitcheva et al. 2003). With relatively few studies, soot structure, i.e., aggregate structure, morphology, substructure and nanostructure remain largely unknown from jet aircraft. As shown here, the variation between the soots from several engine platforms across length scales show that aggregates retained their structure and did not under morphological rearrangement, were not coated nor evidently oxidized. Overall, soots from these aircraft as surveyed are similar in structure to other engine-produced soot, as found by many comparisons in the literature (Song et al. 2006; Vander Wal et al. 2007; Vander Wal and Muller 2006).

Abbreviations

NASA National Aeronautics and Space Administration
TEM   transmission electron microscopy

References

Anderson, B. E., Beyersdorf, A. J., Hudgins, C. H., Plant, J. V., Thornhill, K. L., Winstead, E. L., Ziemba, L. D., Howard, R., Corporan, E., Miake-Lye, R. C., Herndon, S. C., Timko, M., Woods, E., Dodds, W., Lee, B., Santori, G., Whitefield, P., Hagen, D., Lobo, P., Knighton, W. B., Bulzan, D., Tacina, K., Wey, C., Vander Wal, R., Bhargava, A., Kinsey, J., Liscinsky, D. S. (2011). Alternative aviation fuel experiment (AAFEX), NASA/TM—2011-217059, NASA Langley Research Center.

Bisetti, F., Blanquart, G., Mueller, M. E., Pitsch, H. (2012). On the formation and early evolution of soot in turbulent nonpremixed flames. Combust. Flame 159:317-335.

Bond, T. C., Streets, D. G., Yarber, K. F., Nelson, S. M., Woo, J.-H., Klimont, Z. (2004). A technology based global inventory of black and organic carbon emissions from combustion. J. Geophys. Res. 109:D14203-43.

Chakrabarty, R. K. (2008). On the morphology and optics of carbonaceous aerosols. Dissertation of Chemical Physics, University of Nevada.

Colket, M., Edwards, T., Williams, S., Cernansky, N. P., Miller, D. L., Egolfopoulos, F., Seshadri, K., Dryer, F. L., Law, C. K., Friend, D., Lenhert, D., Pitsch, H., Sarofim, A., Smooke, M., Tsang, W. (2007). Development of an experimental database and kinetic models for surrogate jet fuels. 45th AIAA Aerospace Sciences Meeting and Exhibit 8 - 11 January, Reno, Nevada. AIAA 2007-770.

Corporan, E., DeWitt, M. J., Belovich, V., Pawlik, R., Lynch, A. C., Gord, J. R., Meyer, T. R. (2007). Emissions characteristics of a turbine engine and research combustor burning a Fischer-Tropsch jet fuel. Energy Fuels 21:2615-2626.

Demirdjian, B., Ferry, D., Suzanne, J., Popovicheva, O. B., Persiantseva, N. M., Shonija, N. K. (2007). Heterogeneities in the microstructure and composition of aircraft engine combustor soot: Impact on the water uptake. J. Atmos. Chem. 56:83-103.

Dobbins, R. A., Fletcher, R. A., Lu. W. (1995). Laser microprobe analysis of soot precursor particles and carbonaceous soot. Combust. Flame 100:301-309.

Dobbins, R. A., Govatzidakis, G. J., Lu, W., Schwartzman, A. F., Fletcher, R. A. (1996). Carbonization rate of soot precursor particles. Combust. Sci. Technol. 121:103-121.

El-Asrag, H., Lu, T., Law, C. K., Menon, S. (2007). Simulation of soot formation in turbulent premixed flames. Combust. Flame 150:108-126.

El-Asrag, H., Menon, S. (2009). Large eddy simulation of soot formation in a turbulent non-premixied jet flame. Combust. Flame 156:385-395.

Frenklach, M. (2002). Reaction mechanisms of soot formation in flames. PCCP. 4:2028-2037.

Gaddam, C. K., Vander Wal, R. L. (2013). Physical and chemical characterization of SIDI engine particulate. Combust. Flame *(in press)*; DOI: 10.1016/j.combustflame.2013.05.025.

Gangopadhyay, S., Elminyawi, I., Sorensen, C. M. (1991). Optical structure factor measurements of soot particles in a premixed flame. Appl. Opt. 30:4859-4864.

Grieco, W. J., Howard, J. B., Rainey, L. C., Vander Sande, J. B. (2000). Fullerenic carbon in combustion-generated soot. Carbon 38:597-614.

Gudiyella S., Brezinsky K. (2012). High pressure study of n-propylbenzene oxidation. Combust. Flame. 159:940-958.

Gudiyella S., Malewicki T., Comandini A., Brezinsky K. (2011). High pressure study of m-xylene oxidation. Combust. Flame 158:687-704.

Hagen D. E., Whitefield P. D. (1996). Particulate emissions in the exhaust plume form commercial jet aircraft under cruise conditions, J. Geophys. Res.: Atmos. 101:19551-19557.

Herndon, S. C., Onasch, T. B., Frank, B. P., Marr, L. C., Jayne, J. T., Canagaratna, M. R., Grygas, J., Lanni, T., Anderson, B. E., Worsnop, D., Miake-Lye, R. C. (2005). Particulate emissions from in-use commercial aircraft. Aerosol Sci. Tech. 39:799-809.

Howard, J. B, Richter, H. (2000). Formation of polycyclic aromatic hydrocarbons and their growth to soot – a review of chemical reaction pathways. Prog. Energy Combust. Sci. 26:565-608.

Hu, B., Yang, B., Koylu, U. O. (2003). Soot measurements at the axis of an ethylene/air non-premixed turbulent jet flame. Combust. Flame 134:93-106.

Huang, C. H., Vander Wal, R. L. (2013). AAFEX II: Effect of soot structure evolution from commercial jet engine burning petroleum based JP-8 and synthetic HRJ, FT fuels. Energy Fuels *(submitted)*.

ImageJ. (1997). http://rsb.info.nih.gov/ij/

Ishiguro, T., Takatory, Y., Akihama, K. (1997). Microstructure of diesel soot particles probed by electron microscopy: First observation of inner core and outer shell. Combust. Flame 108:231-234.

Karcher, B., Mohler, O., DeMott, P. J., Pechtl, S., Yu, F. (2007). Insights into the role of soot aerosols in cirrus cloud formation. Atmos. Chem. Phys. 7:4203-4227.

Khalizov A. F., Zhang, R., Zhang, D., Xue, H., Pageis, J., McMurry, P. H. (2009). Formation of highly hygroscopic soot aerosols upon internal mixing with sulfuric acid vapor. J. Geophys. Res. 114:D05208.

Kim, W. W., Lienau, J. J., Van Slooten, P. R., Colket, M. B., Malecki, R. E., Syed, S. (2004). Towards modeling lean blow out in gas turbine flameholder applications. J. Eng. Gas Turbines Power 128: 40-48.

Kinsey, J. S., Hays, M. D. (2011). Chemical characterization of the fine particle emissions from commercial aircraft engines during the aircraft particle emissions experiment (APEX) 1 to 3. Environ. Sci. Technol. 45:3415-3421.

Koylu, U. O., Faeth, G. M. (1994). Optical properties of soot in buoyant laminar diffusion flames. J. Heat. Transfer 116:971-979.

Koylu, U. O., Faeth, G. M., Farias, T. L., Garvalho, M. G. (1995). Fractal and projected structure properties of soot aggregates. Combust. Flame 100:621-633.

Li, H., Liu, C., Bi, L., Yang, P., Kattawar, G. W. (2010). Numerical accuracy of equivalent spherical approximations for computing ensemble-averaged properties of fractal soot aggregates. J. Quant. Spectrosc. Radiat. Transfer 111:2127-2132.

Lind, T., Ammar, Y., Dehbi, A., Guntay, S. (2010). De-agglomeration mechanisms of TiO2 aerosol agglomerates in PWR steam generator tube rupture conditions. Nucl. Eng. Des. 240: 2046-2053.

Liu, F., Smallwood, G. J. (2009). Radiative properties of numerically generated fractal soot aggregates: The importance of configuration averaging. J. Heat Transfer 132:023308-023313.

Merchan-Merchan, W., Sanmiguel, S. G., McCollam, S. (2012). Analysis of soot particles derved from biodiesels and diesel fuel air-flames. Fuel 102:525-535.

Penner J. E., Lister D. H., Griggs D. J., Dokken D. G. J., McFarland M. (1999). Aviation and the Global Atmosphere, Intergovernmental Panel on Climate Change Rept., Cambridge Univ. Press, Cambridge, England, U.K., p. 373.

Popovitcheva, O., Persiantseva, N. M., Kuznetsov, B. V., Rakhmanova, T. A., Shonija, N. K., Suzanne, J., Ferry, D. (2003). Microstructure and water adsorbability of aircraft combustor soots and kerosene flame soots: Toward an aircraft-generated soot laboratory surrogate. J. Phys. Chem. A 107:10046-10054.

Popovitcheva, O., Persiantseva, N. M., Trukhin, M. E., Rulev, G. B., Shonija, N. K., Buriko, Y. Y., Starik, A. M., Demirdjian, B., Ferry, D., Suzanne, J. (2000). Experimental characterization of aircraft combustor soot: Microstructure, surface area, porosity and water adsorption. PCCP. 2:4421-4426.

Puri, R., Richardson, T. F., Santoro, R. J. (1993). Aerosol dynamic processes of soot aggregates in a laminar ethane diffusion flame. Combust. Flame 92:320-333.

Raj, A., Man, R. L. W., Totton, T. S., Snader, M., Shirley, R. A., Kraft, M. (2010). New polycyclic aromatic hydrocarbon (PAH) surface processes to improve the model prediction of the composition of combustion generated PAHs and soot. Carbon 48:319-332.

Riemer, N., Vogel, H., and Vogel, B. (2004). Soot aging time scales in polluted regions during day and night. Atmos. Chem. Phys. 4:1885-1893.

Santoro, R. J., Semerjian, H. G., Doblins R. A. (1983). Soot particle measurements in diffusion flames. Combust. Flame 51:203-218.

Schmid O., Hagen, D., Whitefield, P. D., Trueblood, M. B., Rutter, A. P., Lilenfeld, H. V. (2004). Methodology for particle characterization in the exhaust flows of gas turbine engines. Aerosol Sci. Tech. 38:1108-1122.

Shim, H.-S., Hurt, R. H., Yang, N. C. (2000). A methodology for analysis of 002 lattice fringe images and its application to combustion-derived carbons. Carbon 38:29-45.

Slowik, J. G., Stainken, K., Davidovits, P., Williams, L. R., Jayne, J. T., Kolb, C. E., Worsnop, D. R., Rudich, Y., DeCarlo, P. F., Jimenez, J. L. (2004). Particle morphology and density characterization by combined mobility and aerodynamic diameter measurement. Part 2: Application to combustion-generated soot aerosols as a function of fuel equivalence ratio. Aerosol Sci. Technol. 38:1206-1222.

Song, J., Alam, M., Boehman, A. L., Kim, U. (2006). Examination of the oxidation behavior of biodiesel soot. Combust. Flame 146:589-604.

Teini, P. D., Karwat, D. M. A., Atreya, A. (2011). Observations of nascent soot: Molecular deposition and particle morphology. Combust. Flame 158:2045-2055.

Timko, M. T., Yu, Z., Onasch, T. B., Wong, H.-W., Miake-Lye, R. C., Beyersdorf, A. J., Anderson, B. E., Thornhill, K. L., Winstead, E. L., Corporan, E., DeWitt, M. J., Klingshirn, C. D., Wey, C., Tacina, K., Liscinsky, D. S., Howard, R., Bhargava, A. (2010). Particulate emissions of gas turbine engine combustion of a Fischer-Tropsch synthetic fuel. Energy Fuels 24:5883-5896.

Tolpadi, A. K., Correa, S. M., Burrus, D. L., Mongia, H. C. (1997). Monte carlo probability density function method for gas turbine combustor flowfield predictions. J. Propul. Power 13:218-225.

Vander Wal, R. L. (1997). LIF-LII measurements in a turbulent gas-jet flame. Exp. Fluids 23:281-287.

Vander Wal, R. L. (1998). Soot precursor carbonization: Visualization using LIF and LII and comparison using bright and dark field TEM. Combust. Flame 112:607-616.

Vander Wal, R. L., Bryg, V. M. (2013). Chemistry characterization of jet aircraft engine particulate by XPS: results from APEX III. Aerosol Sci. Technol. (submitted).

Vander Wal, R. L., Bryg, V. M., Huang, C. H. (2013). Aircraft engine particulate: Macro- micro- and nanostructure by HRTEM and Chemistry by XPS. Combust. Flame (submitted).

Vander Wal, R. L., Jensen, K. A., Choi, M. Y. (1997). Simultaneous laser-induced emission of soot and polycyclic aromatic hydrocarbons within a gas-jet diffusion flame. Combust. Flame 109:399-414.

Vander Wal, R. L., Lee, K. O., Choi, M. Y. (1995). The effects of rapid heating of soot: Implications when using laser-induced incandescence for soot diagnostics. Combust. Flame 102:200-204.

Vander Wal, R. L., Mueller, C. J. (2006). Initial investigation of effects of fuel oxygenation on nanostructure of soot from a direct-injection diesel engine. Energy Fuel 20:2364-2369.

Vander Wal, R. L., Tomasek, A. J. (2003). Soot oxidation: Dependence upon initial nanostructure. Combust. Flame 134:1-9.

Vander Wal, R. L., Tomasek, A. J., Street, K., Hull, D. R., Thompson, W. K. (2004). Carbon nanostructure examined by lattice fringe analysis of high-resolution transmission electron microscopy images. Appl. Spectrosc. 58:230-237.

Vander Wal, R. L., Yezerets, A., Currier, N. W., Kim, D. H., Wang, C. M. (2007). HRTEM study of diesel soot collected from diesel particulate filters. Carbon 45:70-77.

Wey, C. C., Anderson, B. E., Hudgins, C., Wey, C., Li-Jones, X., Winstead, E., Thornhill, L. K., Lobo, P., Hagen, D., Whitefield, P., Yelvington, P. E., Herndon, S. C., Onasch, T. B., Miake-Lye, R. C., Wormhoudt, J., Knighton, W. B., Howard, R., Bryant, D. (2006). Aircraft particle emissions experiment (APEX), NASA TM-2006-214382.

Wey, C. C., Anderson, B. E., Wey, C., Miake-Lye, R. C., Whitefield, P., Howard, R. (2007). Overview on the aircraft particle emission experiment. J. Propul. Power 23:898-905.

Wuebbles, D., Gupta, M., Ko, M. (2007). Evaluating the impacts of aviation on climate change. EOS, Trans. Am. Geophys. Union 88:157-168.

Yehliu, K. (2010). Impacts of Fuel Fromulation and Engine Operating Parameters on the Nanostructure and Reactivity of Diesel Soot. Desrtation of Energy and Mineral Engineering, Pennsylvania State Univeristy.

Yehliu, K., Vander Wal, R. L., Boehman, A. L. (2011). Development of an HRTEM image analysis method to quantify carbon nanostructure. Combust. Flame 158:1837-1851.

Zhang, Y., Boehman, A. L. (2013). Oxidation behavior of soot generated from the combustion of methyl 2-butenoate in a co-flow diffusion flame. Combust. Flame 160:112-119.

Zhu, J., Lee, K. O., Yozgatligil, A., Choi, M. Y. (2005). Effects of engine operating conditions on morphology microstructure, and fractal geometry of light-duty diesel engine particulates. P. Combust. Inst. 30:2781-2789.